Accepted Manuscript

Synthesis of finest superparamagnetic carbon-encapsulated magnetic nanoparticles by a plasma expansion method for biomedical applications

Lavita Sarma, N. Aomoa, Trinayan Sarmah, S. Sarma, A. Srinivasan, G. Sharma, Ajay Gupta, V.R. Reddy, B. Satpati, D.N. Srivastava, S. Deka, L.M. Pandey, M. Kakati

PII: S0925-8388(18)31132-0

DOI: 10.1016/j.jallcom.2018.03.261

Reference: JALCOM 45491

To appear in: *Journal of Alloys and Compounds*

Received Date: 17 January 2018

Revised Date: 19 March 2018

Accepted Date: 21 March 2018

Please cite this article as: L. Sarma, N. Aomoa, T. Sarmah, S. Sarma, A. Srinivasan, G. Sharma, A. Gupta, V.R. Reddy, B. Satpati, D.N. Srivastava, S. Deka, L.M. Pandey, M. Kakati, Synthesis of finest superparamagnetic carbon-encapsulated magnetic nanoparticles by a plasma expansion method for biomedical applications, *Journal of Alloys and Compounds* (2018), doi: 10.1016/j.jallcom.2018.03.261.

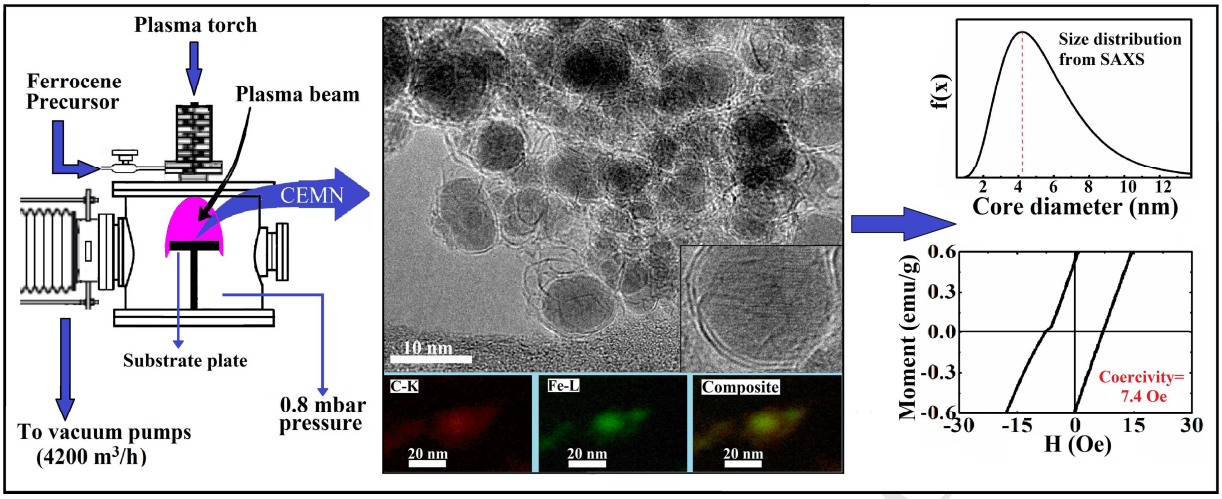

Synthesis of finest superparamagnetic carbon-encapsulated magnetic nanoparticles by a plasma expansion method for biomedical applications

Lavita Sarma[a], N. Aomoa[a], Trinayan Sarmah[a], S. Sarma[b], A. Srinivasan[b], G. Sharma[c], Ajay Gupta[c], V.R. Reddy[d], B. Satpati[e], D.N. Srivastava[f], S. Deka[g], L.M. Pandey[g], M. Kakati[a,*]

[a]*CIMPLE-PSI Laboratory, Centre of Plasma Physics-Institute for Plasma Research, Sonapur 782402, Assam, India*
[b]*Department of Physics, Indian Institute of Technology, Guwahati 781039, Assam, India*
[c]*Amity Centre for Spintronic Materials, Amity University, Noida 201313, Uttar Pradesh, India*
[d]*UGC-DAE Consortium for Scientific Research, Khandwa Road, Indore 452017, Madhya Pradesh, India*
[e]*Saha Institute of Nuclear Physics, 1/AF Bidhan Nagar, Kolkata 700064, West Bengal, India*
[f]*CSIR-Central Salt & Marine Chemicals Research Institute, Takhteshwar, Bhavnagar 364002, Gujarat, India*
[g]*Department of Biosciences & Bioengineering, Indian Institute of Technology, Guwahati 781039, Assam, India*

*Corresponding author.
E-mail address: mayur@cppipr.res.in (Mayur Kakati), Phone: +919435036180

Abstract

This paper demonstrates fine size-controlled synthesis of superparamagnetic carbon-encapsulated iron nanoparticles, by a supersonic plasma jet assisted rapid, bulk-production process, by manipulation of the pressure in the sample collection chamber. Transmission electron microscopy and small angle x-ray scattering measurements confirmed the formation of single-crystals with a narrow size distribution, having core average size of 5.0 nanometer and encapsulated by an ultrathin carbon coating, for sub-mbar pressure. VSM and Mossbauer characterization established the nanocrystallites to be superparamagnetic in nature, with saturation magnetization 67 emu/g and coercive field 7.4 Oe. Controlled plasma heating during synthesis led to the burning down of extra carbon that resulted in further enhancement of the magnetization of the product. Graphitization of the encapsulating layers also enhanced, which could successfully protect the metallic core from oxidation, as well as improved its cyto-compatibility. This purified sample could be ideal for targeted drugs delivery and water treatment applications. Another sample was processed through controlled reaction with oxygen, the as-synthesized sample having magnetic properties approaching that of the first sample, which may be more attractive especially for water treatment processes because of the simpler single-step processing of the material.

(Keywords: Carbon Encapsulated Magnetic Nanoparticles, Plasma processing, Superparamagnetic properties, Mossbauer spectroscopy, Small Angle X-ray Scattering)

1. Introduction

Magnetic nanoparticles protected by encapsulating carbon layers offer vast application potential especially in the fields of biomedicine and environmental engineering [1-3]. The surface of a superparamagnetic nanoparticle can be loaded with drugs, which may be then manipulated with an external magnetic field for targeted delivery to a cancerous tumor [1]. Superparamagnetic properties, in this case, ensure that there is no dangerous aggregation of particles inside the anatomical systems once the magnetic field is removed. Carbon encapsulated magnetic nanoparticles (CEMN) can be also employed to detect cancerous cells through magnetic resonance imaging and to kill the malignant cells through hyperthermia using an alternating magnetic field [1]. Superfine magnetic particles have been highlighted for application in water and wastewater treatment, where also superparamagnetism has been pointed out as an essential property for efficient performance [2]. The very small coercive field will allow easy separation of the magnetic particles from water by a small magnetic field, while the shell will absorb the heavy metals and other pollutants [4]. In CEMN, the protecting carbon shell has the advantage of being light in weight, stable in physiological and high-temperature environments, biocompatible, which can be easily functionalized to carry drugs over its surface. Various techniques have been used for the synthesis of CEMN such as chemical vapor deposition [5], pyrolysis [6], combustion [7], DC thermal plasma synthesis [8], arc discharge synthesis, [9], pulse laser irradiation [10] and RF plasma torch [11]. Plasma-assisted methods, in general, have the advantage of bulk productivity and fine crystallinity of the product materials [8].

Size-controlled synthesis is the vital issue here, because CEMN smaller than the corresponding domain sizes (15 nm for iron) only may demonstrate superparamagnetic behavior [12-16]. It is therefore important to be able to synthesize smallest sizes with an essentially narrow dispersion, because the product may demonstrate the smooth variation of their magnetic properties with size only when individual samples are synthesized with sufficiently narrow size distribution. Nanoparticles with poly-dispersed sizes have a larger tendency to aggregate with each-other [17]. A thin size distribution favors dispersion stability that may be an important issue for all the intended applications with this nanomaterial [18].

In a previous communication, we had demonstrated synthesis of CEMN by an expanded thermal plasma assisted process, where average size and size distribution were controlled simply by manipulation of the ambient pressure in the sample collection chamber [8]. The average particle size and corresponding coercive fields were seen decreasing continuously upon lowering the chamber pressure. However, corresponding to the minimum pressure of 20 mbar the coercive field was more than 50 Oe, which is not strictly considered as the characteristic of the superparamagnetic material. In this communication, we have attempted

the further reduction of CEMN sizes by enhancing the vacuum pumping capability of the experimental system and carried out elaborate characterization of the product nanocrystals. Along with Transmission Electron Microscopy (TEM), we have used the technique of Small Angle X-ray Scattering (SAXS) for measurement of the size distribution of the product, where the later has the advantage of being more accurate because sampling is done over a much larger volume of the sample.

The intended use of CEMN in biomedicine will inevitably lead to direct interaction with humen and other living systems. Therefore, we tested the cyto-compatibility of the synthesized materials in the wide range (0.2 to 10.0 mg/ml) against mouse fibroblast cell line L929, using MTT (3-(4, 5-Dimethylthiazol-2-Yl)-2, 5-Diphenyltetrazolium Bromide) assay to examine its suitability for the intended biomedical applications. The University of Warsaw, Poland group who pioneered plasma synthesis of carbon encapsulated iron nanoparticles, also had first initiated biocompatibility studies for their product nanomaterials [19]. I.P. Grudzinski *et al.*, had undertaken an elaborate study, using different cell lines like human melanoma, mouse melanoma and human dermal fibroblast, and four different assays [20]. In another significant study, the same author explored cytotoxic response of the murine glioma cells using surface functionalized carbon encapsulated iron nanoparticles. The results suggested that the toxic response depends on the amount of the nanomaterial administered and especially on the surface functionalization of the
encapsulated powders [21].

2. Experimental

2.1. Supersonic thermal plasma assisted reactor configuration and synthesis of CEMN

A segmented DC plasma torch assisted experimental reactor was used for the synthesis experiments (Fig.S1, supplementary materials), where superfine particles nucleate during supersonic expansion cooling of the plasma jet laden precursors through a converging nozzle into a bottom vacuum chamber, details of which are available elsewhere [22]. To reduce ambient pressure in the sample collection chamber further, a high throughput roots vacuum pump (EH 4200 backed with an E2M 275 rotary vacuum pump) was employed in this experiment, which produced 0.8 mbar pressure. Argon was injected at the cathode at 20 liters per minute (lpm) using a digital mass flow controller (Alborg make), and plasma operated at 150 Amp current (8.7 kW). Using a Tubular furnace ferrocene ($FeC_{10}H_{10}$, Spectrochem, 98% purity) vapor was injected into the plasma at 31g/h for 8 minutes, carried by 5 lpm hydrogen. The product powders were deposited on all exposed parts inside the chamber and produced a thick coating within a few minutes of operation. As synthesized samples (designated as CEMN-AS) were collected from a substrate kept at a distance of 120 mm from the reactor nozzle, where it deposited at a rate of 3.36 g/h that corresponds to a yield of 10.6 %. Total power consumed during synthesis is 4.123 kWh (including torch, pumps, water cooling, etc: 31 kW*0.133 h = 4.123 kWh) for the production of 0.447g sample. Thus the energy consumed per one gram of the product is 9.2 kWh. Parts of the samples were purified by aqua-regia,

prepared by mixing three parts of hydrochloric acid with one part of nitric acid by volume. Raw samples were mixed with the acid and kept for 3h, after which it was diluted with distilled water and filtered. The residue in the filter paper was first washed with distilled water and then with acetone into a beaker. Samples were attracted to the bottom of the beaker with a permanent magnet and excess acetone was discarded, which was then dried in vacuum, and stored for later characterization. The final purified is designated as CEMN-P. The purification yield was found as 40%.

2.2. Nanomaterial characterization methods

For morphological and compositional analysis of the samples, we used a JEOL, JEM 2100 HRTEM system (200 kV) and an FEI, Tecnai G^2 F30, S-Twin TEM (300 kV) equipped with a Gatan imaging filter (model 963). The later had an Energy Dispersive X-ray (EDX) spectroscope attached for elemental analysis. The material phases and the degree of crystallinity of the carbon were deduced by X-ray Diffraction (XRD, Rigaku TTRAX-III, 5kW, λ=1.5406Å, 2θ-range: 20° to 60°, step: 0.02, at a scan rate of 2 deg s^{-1}) and Laser Mirco-Raman (LabRam HR, Horiba-Jobin Yvon, Argon laser, 488 nm) techniques. Small-angle x-ray scattering (SAXS) measurements were also undertaken in transmission geometry at micro and nano focus x-ray scattering (MiNaXS) beamline P03 of PETRA III synchrotron radiation source, Hamburg, Germany (13 keV X-rays, PILATUS 1M detector). This also provided size information in addition to the HRTEM. For fitting the SAXS experimental data, the iron core was modeled as covered by a carbon shell. The data was analyzed by SASFIT software, by taking the spherical iron core to have a lognormal size distribution with average size and width of distribution taken as fitting parameters. The electron density of carbon shell and its width were taken as other fitting parameters. The magnetization (M-H loop) of the sample at room temperature and the temperature dependence of magnetization at the constant applied magnetic field of 500 Gauss were studied by vibrating sample magnetometer (VSM, Lake Shore 7410). The different iron-containing phases were explored at room temperature and at 5K, by Mossbauer spectroscopy in transmission geometry at zero applied external magnetic field, where a constant acceleration spectrometer was used with ^{57}Co radioactive source. Thermogravimetric analysis (TGA, STA7200, Hitachi, performed in oxygen, heated up to 800 $^{\circ}$C at the scan rate of 5°/min) was also performed to estimate the carbon contents of samples.

2.3 Measurement of the cytotoxicity of the product material

The *in-vitro* cyto-compatibility tests were performed for the synthesized CEMN samples on mouse fibroblast cell line L929, using MTT (3-(4, 5-Dimethylthiazol-2-Yl)-2, 5-Diphenyltetrazolium Bromide) assay, using procedures described previously [23]. The L929 cell line was cultured in Dulbecco's modified Eagle's medium with 10% fetal calf serum at 37°C at 5% CO_2. In order to perform the MTT assay, 10^4 cells/100 µl were seeded in each well of 96 well culture plates and incubated with a varying amount of sample powders (20, 40, 80, 160, 500 and 1000 µg) for 24 hours at 37°C. After the incubation period, media was replaced with fresh 100 µl media containing 10 µl of MTT solution (5mg/ml, PBS pH 7.4)

and incubated for 4 hours at 37 ºC. After 4 hours the media was removed completely and 150 µl DMSO was added to each well followed by incubation for another 10 minutes in order to dissolve the formazan crystals. The absorbance of each well was recorded at 570 nm (Infinite 200 Pro, Tecan). The metabolic activity of live cells was characterized by the formation of formazan crystals. The OD values of positive control (cells incubated without samples) were considered as 100% to compare with OD of the samples incubated with synthesized samples. The percentage of cell viability was calculated from the ratio, the optical density (OD) values of cells incubated with samples (Sample Intensity) and OD values of the cells incubated without samples (Control Intensity).

3. Results and discussions

3.1. Transmission electron Microscope (TEM) analysis

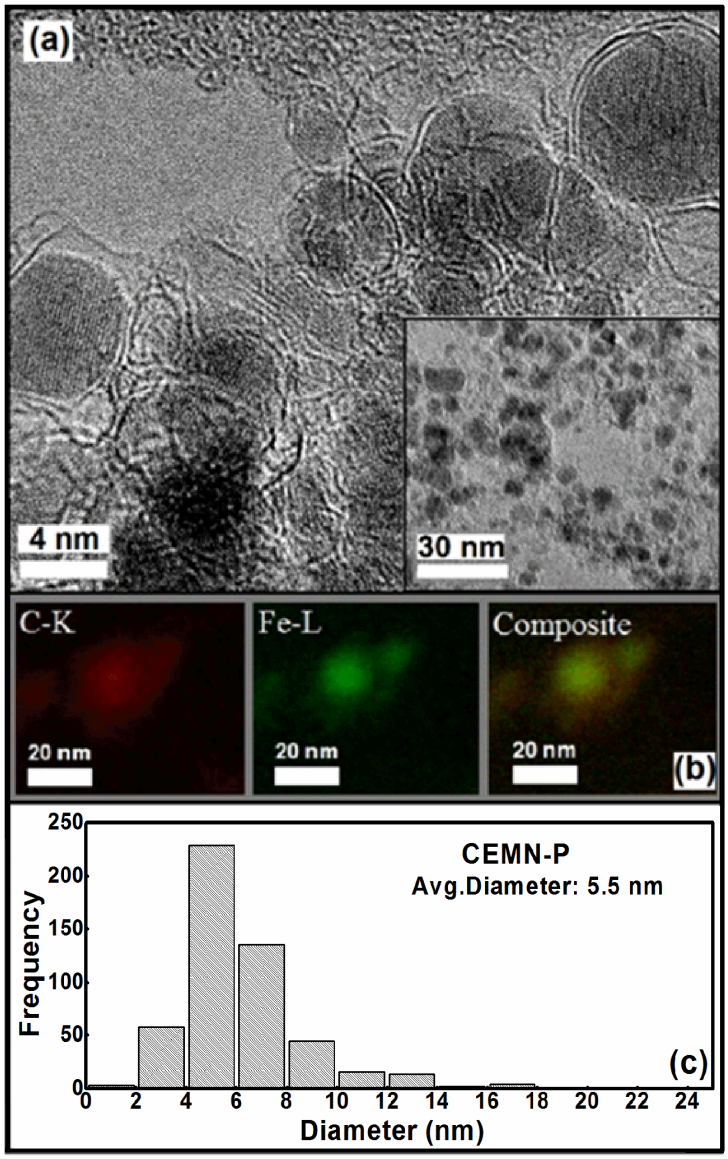

Fig.1. (a) HRTEM image of the purified carbon-encapsulated magnetic nanoparticles (CEMN–P), TEM image of the same in the inset (b) EFTEM images of C, Fe and composite image (CEMN–P) (c) core size-distribution of the same sample (CEMN–P).

HRTEM and TEM images (Fig.1a) of the purified sample (CEMN-P) show single-crystal-like superfine nanoparticles encapsulated by one or two typical layers of carbon. Energy filtered TEM (EFTEM) (Fig.1b) imaging also reconfirms formation of core-shell structures, with an iron core surrounded by carbon shells. The sample appeared to be perfectly homogeneous, CEMN dispersed in a carbon matrix, but devoid of any unreacted micron-sized particles. Size distribution of the nanoparticles (CEMN-P) was constructed by considering total 507 numbers of particles from 3 numbers of corresponding TEM micrographs (Fig.1c), which gives the average size of 5.5 nanometers. This is the smallest size for CEMN synthesized by any method to the best of our knowledge. Considering the size distribution as Gaussian, the corresponding standard deviation is estimated at 1.5 nm, which again is the narrowest compared to our previous CEMN samples synthesized at relatively higher pressure [8]. Twin planes or stacking faults are also seen in some well-resolved HRTEM photographs, which are suspected to be γ-Fe because such faults are usually observed in FCC phases only [3].

3.2 XRD and Raman measurement

The as-synthesized CEMN sample contained little oxides, which was successfully eliminated in the purified sample as confirmed by the corresponding XRD pattern (Fig.2a). However, continuing the previous trend, the XRD peaks as observed in the earlier work, viz., α-Fe, Fe_3C, γ-Fe/γ-Fe(C) all merged together for this sample with the smallest particle sizes so far. The prominent SAED rings identified to be associated with the following crystal planes supported the same phase composition: (110) plane of α-Fe/ (102) of Fe_3C, (210) plane of Fe_3C and (211) of α-Fe (figure not presented in the manuscript). Crystal lattice inter-planar distance was measured from HRTEM photographs as 2.06 A°, which also correspond to (110) plane of α-Fe or (102) plane of Fe_3C (figure not presented in the manuscript). EDX confirmed that nanocrystallites were free from any impurities (figure not presented in the manuscript). Raman measurements demonstrated that the ratio of the intensity corresponding to the G (1589 cm^{-1}) and D (1346cm^{-1}) Raman bands (I_G/I_D) were 1.02 and 1.5 for the as-synthesized (CEMN-AS) and the purified (CEMN-P) sample respectively (Fig.2b). The Raman spectra were de-convoluted and the integral areas of the de-convoluted G and D bands were taken into consideration. The Raman spectra were first normalized before calculation of integrated area using Lorentzian fitting. The results indicate that the carbon content of the purified sample was better graphitized compared to our previous samples [8].

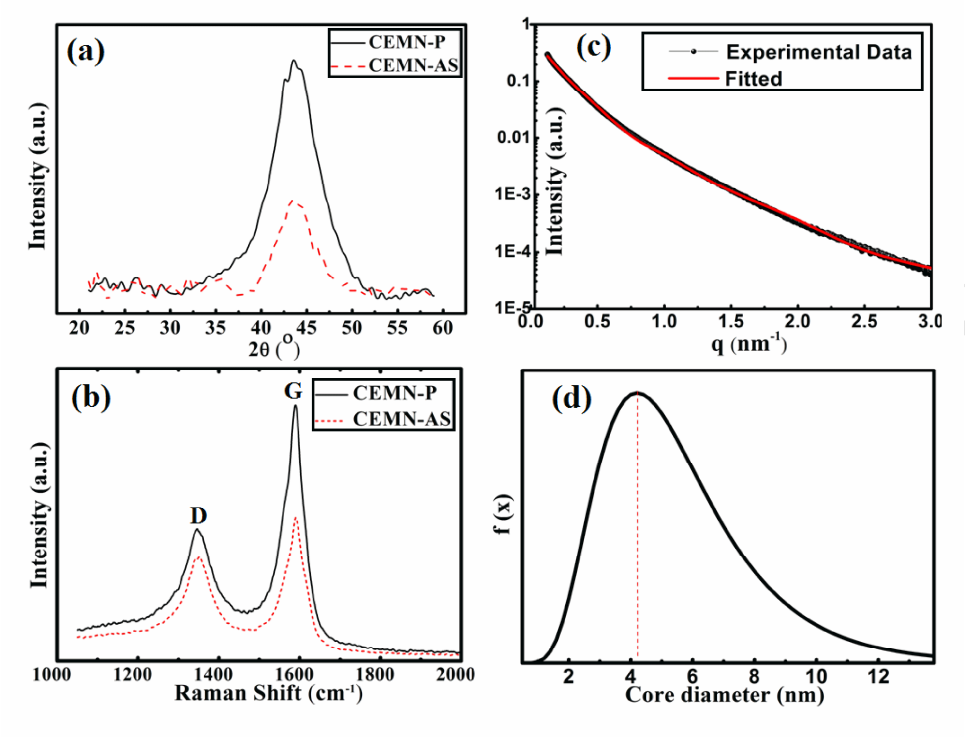

Fig.2. (a) XRD and (b) Raman spectra of CEMN-AS and CEMN-P samples (c) fitted SAXS data of CEMN-P (d) SAXS measured size distribution of particles (CEMN-P).

3.3. Small Angle X-ray Scattering analysis

The curve in Fig.2c gives fitting of SAXS experimental data (CEMN-P) that also led to the determination of the size distribution of the core magnetic nanoparticles as depicted in Fig.2d, with an average size of 5.0 nm and thickness of the carbon shell as 0.2 nm. This is in agreement with the previous HRTEM measurements that the CEMN are covered with an ultrathin graphene layer. Significantly, both of the measurements demonstrate that the size distribution was skewed towards larger sizes. The mass density of carbon was measured through simulation as 2.0 ± 0.05 gm/cm^3. A good correlation between sp^3 content and the mass density had been observed before for carbon materials, that is available in the literature [24]. In the present case, a mass density even lower than that of graphite suggests a strong sp^2 content that is in qualitative agreement with the Raman results [24].

3.4 Vibrating sample magnetometer (VSM) and Mossbauer spectroscopy analysis

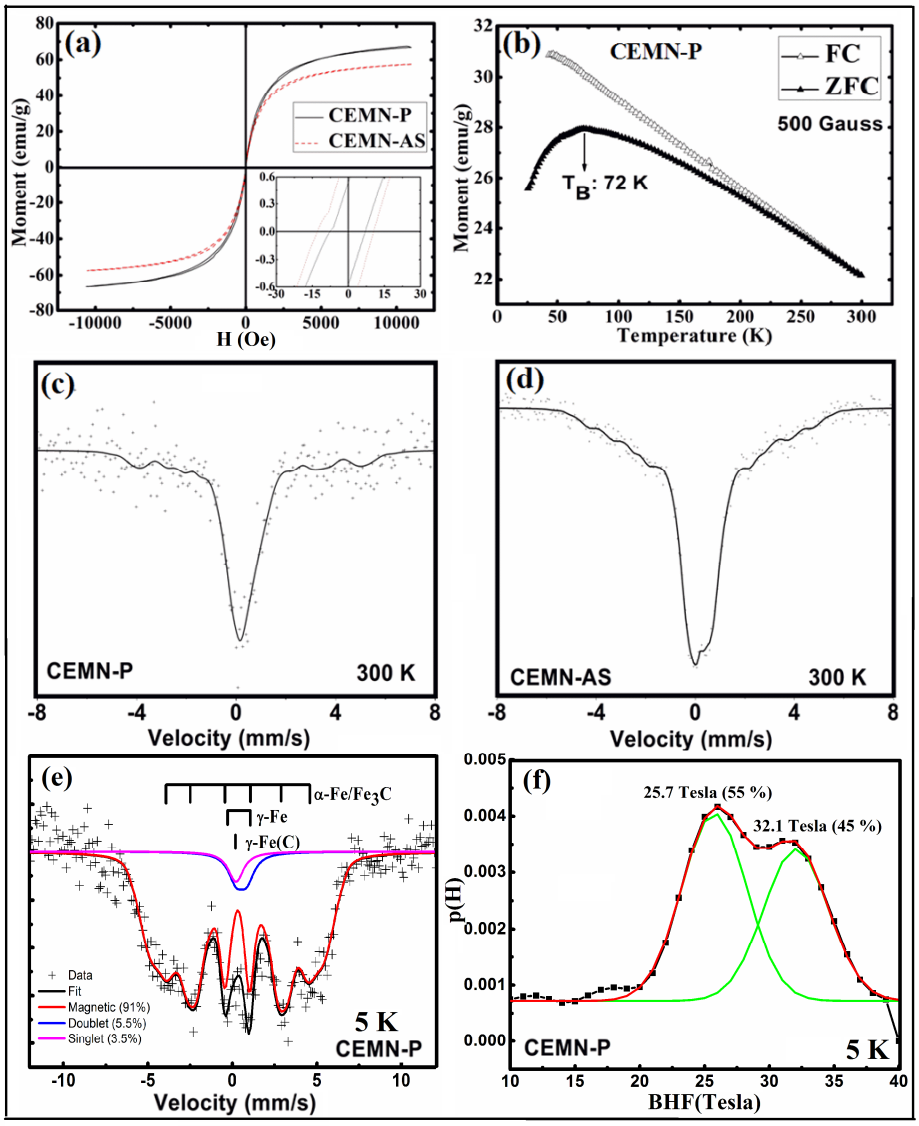

Fig.3. (a) VSM measured magnetic hysteresis loop of CEMN-AS and CEMN-P at room temperature, (b) thermo magnetization data showing FC and ZFC curves for CEMN-P, Mossbauer spectra for (c) CEMN-P at 300K (d) CEMN-AS at 300K, (e) CEMN-P at 5K and (f) hyperfine field distribution for CEMN-P at 5K.

The saturation magnetization (M_s) and coercive field (H_c) for the as-synthesized sample (CEMN-AS) were measured by VSM as 57.7emu/g and 11.8 Oe respectively, which enhanced to 67 emu/g and 7.4 Oe for the purified particles (CEMN-P, Fig.3a). To our knowledge, this is the smallest coercive field measured for CEMN synthesized by any method so far, which may be conveniently termed as superparamagnetic material. The zero field cooled (ZFC) and field cooled (FC) curves depicted in Fig.3b show a deviation below room temperature. From the position of the peak in the ZFC curve, the blocking temperature (BT), below which the thermally induced spin fluctuation is frozen for the single domain particle, was calculated to be 72 K. Low BT of the CEMN ensures its superparamagnetic behavior under any

physiological conditions. The superparamagnetic nature of the CEMN will allow its easy separation/recovery under a low-gradient magnetic field as well as reusability. This endorses its suitability for the various biomedical applications i.e. targeted drug delivery and hyperthermia etc. and environmental applications i.e. water and waste water treatment. Important properties of these samples are recorded in Table 1.

Table 1

Saturation magnetization (Ms), coercive field (Hc), remnant magnetization (Mr) and other important parameters of the CEMN samples.

Sample name	M_s (emu/g)	H_c (Oe)	M_r (emu/g)	Ratio of I_G/I_D	Average particle Size (nm)
CEMN-AS	57.7	11.7	0.96	1.02	Not available
CEMN-P	67	7.4	0.55	1.5	5.5 (TEM), 5.0 (SAXS)

Room temperature ^{57}Fe Mossbauer measurements show a small collapsing sextet for CEMN-P (Fig.3c) and a predominant doublet for CEMN-AS (Fig.3d). The former converts into a broad sextet at low temperature (5K), which actually demonstrates superparamagnetic relaxation of the sample at a relatively high temperature (Fig.3e). The 5K Mossbauer data is fitted with the distribution of hyperfine fields and the obtained hyperfine fields viz., 25.7 and 32.1 Tesla reconfirm the presence of the Fe_3C and α-Fe phases and complete elimination of the iron oxides (Fig.3f). One singlet and one doublet corresponding to the nonmagnetic γ-Fe and γ-Fe(C) were also identified, which together were estimated to constitute about 9% of the total. Of the remaining 91% that was magnetic, the α-Fe phase was about 45%, while the rest was in Fe_3C phase. This is largely in agreement with the Mossbauer studies by Borysiuk *et al.*, who had before identified large presence of Fe_3C and γ-Fe/γ-Fe(C) phases in addition to α-Fe, in CEMN synthesized by arc plasma assisted processes [9].

In this reactor configuration, the precursors embedded in the plasma jet undergo uniform, rapid cooling while supersonically expanding into the low-pressure sample collection chamber, which ensures gas phase condensation of superfine particles with narrow size distribution [22]. Carbon remains dissolved in iron, which subsequently segregates to the surface forming complete encapsulation, as the particles accelerate in the downwards direction [8]. In this present experiment, in continuation of the trend seen before, the average size (and coercive fields) of the magnetic core had decreased further with reduction of pressure in the sample collection chamber [8]. This is due to the higher rate of cooling as experienced by the precursors and less aggregation of particles after nucleation as a result of the lower pressure in the particle growth region. Moreover, the surface carbon layer achieved in this experiment was one of the thinnest reported so far, which was a direct consequence of the very small sizes of the core particles. This is because the superfine particle had a very large specific surface area, the total dissolved carbon, in this case, was sufficient for forming just one or two surface layers only. However, they could provide sufficient protection both against oxidation and acid

during the purification process. During water treatment by CEMN, the core magnetic nanoparticle may act as the reducing agent for inorganic as well as organic pollutants, where an ultrathin protecting shell will ensure that the reactivity of the metal does not get seriously reduced [25]. However, in contrast to the trend observed before [8], the saturation magnetization of the CEMN had enhanced further with reduction of pressure. This is due to the efficient elimination of the background carbon matrix by the under-expanded plasma beam configuration that formed in this lowest pressure regime, which had engulfed the substrate and burnt down the mixed carbon. This is supported by TGA measurement which shows 54% carbon in the CEMN-P sample (Fig.4) as compared to 62% in the sample synthesized at 20 mbar pressure previously [8]. However, the substrate heating resulted in very small CEMN growing into carbon nanotubes that may be considered as a minor impurity in the product nanomaterial (figure not presented in the manuscript). The very small particles in the sample, which usually does not get encapsulated, started acting as classical catalyst nanoparticles, i.e. catalyzing the growth of single-walled nanotubes once deposited on the heated substrate.

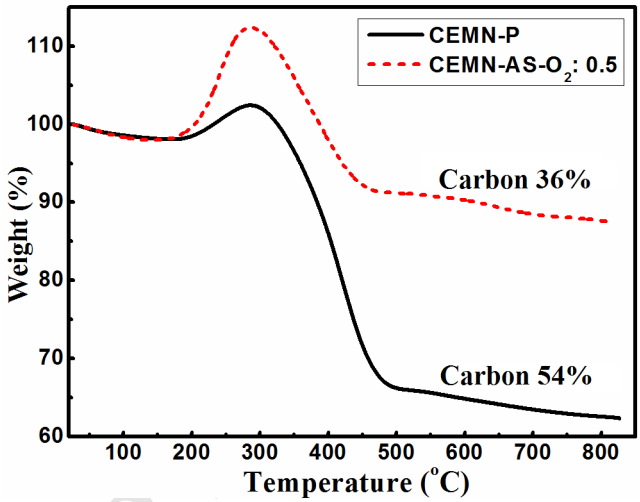

Fig.4. Thermo-Gravimetric Analysis for CEMN-P and CEMN-AS-O_2:0.5.

We had carried out few additional experiments for further reduction of mixed carbon by controlled reaction with oxygen, by injecting O_2 *in-situ* in the vacuum chamber, at 0.5, 1, 2 and 5 lpm respectively. Best results were achieved for the lowest O_2 flow rate (0.5 lpm), where *Ms* of the as-synthesized sample (CEMN-AS-O_2:0.5) had enhanced to 67 emu/g (H_c=8.0 Oe), compared to 57 emu/g (H_c=11.7 Oe) for CEMN-AS (Fig.5a). This must be due to the further elimination of carbon, confirmed later by TGA showing carbon reduced to 36% for this as-synthesized sample (Fig.4).

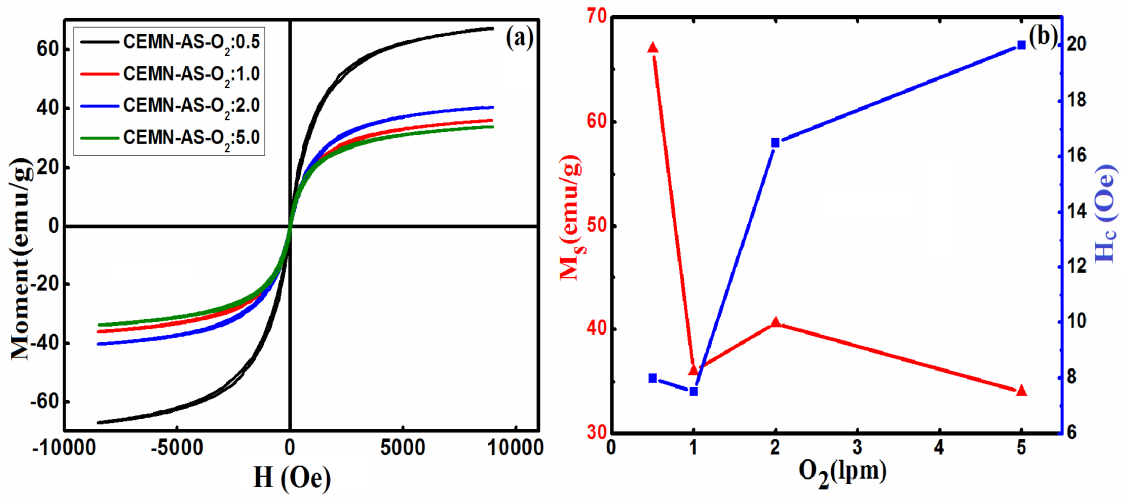

Fig.5. (a) VSM curve for as-synthesized CEMN samples on injection of oxygen into the vacuum chamber at 0.5, 1, 2 and 5 lpm (b) Variation of magnetic saturation and coercive-field with respect to oxygen injection at 0.5, 1, 2 and 5 lpm.

In case of the corresponding purified sample (CEMN-P-O_2:0.5), the post-treatment of the particles through aqua-regia had converted the surface layers into graphene-oxide (GO). XRD (Fig.6a) of the sample shows GO peaks, Raman of which confirms their reduced crystallinity (Fig.6b), because of which the purified sample did not have sufficient stability. All other high oxygen flow rate processed samples were badly oxidized with inferior magnetic properties (Fig.6c). Magnetic characteristics of CEMN-AS-O_2:0.5 were comparable to CEMN-P, but it contained oxide impurity phases. However, this sample has the advantage of being processed by a single step process, hence may be most suitable for water treatment like applications, which demands a high rate of production through a relatively simpler process. The production rate of the reactor used in this experiment was 3.36g/h. The minimum and maximum production yield reported by M. Bystrzejewski et al [13] in supplementary data is 7% and 50% respectively. The maximum production rate reported by them is 240g/h.

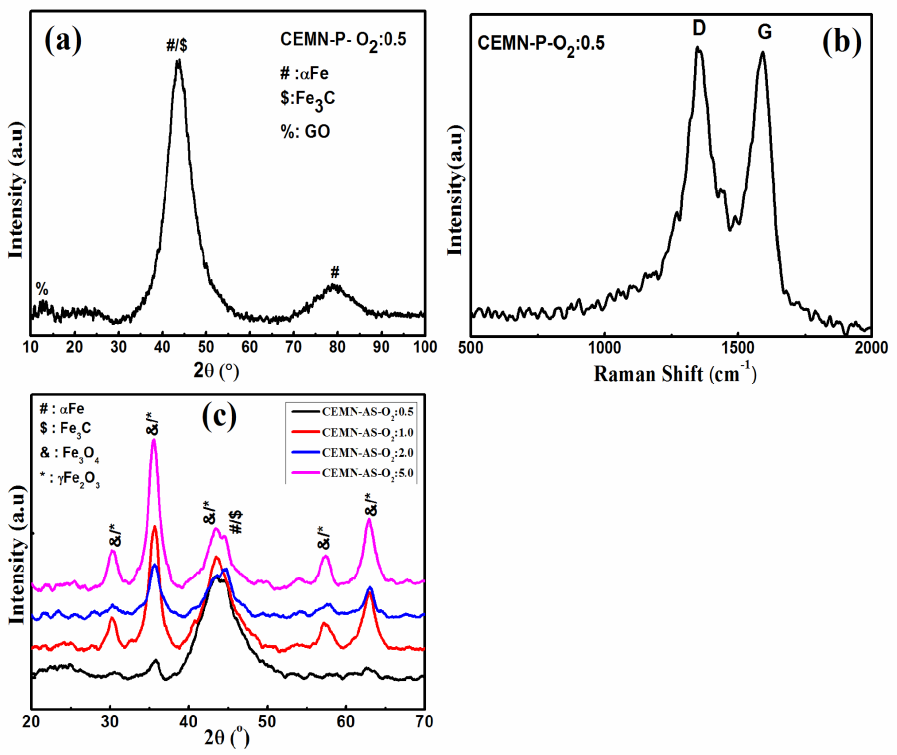

Fig.6. (a) XRD of CEMN-P-O_2:0.5, (b) Raman spectra of CEMN-P-O_2:0.5 and (c) XRD for as-synthesized samples on injection of oxygen into the vacuum chamber at 0.5, 1, 2 and 5 lpm.

3.5 Measurement of cytotoxic properties

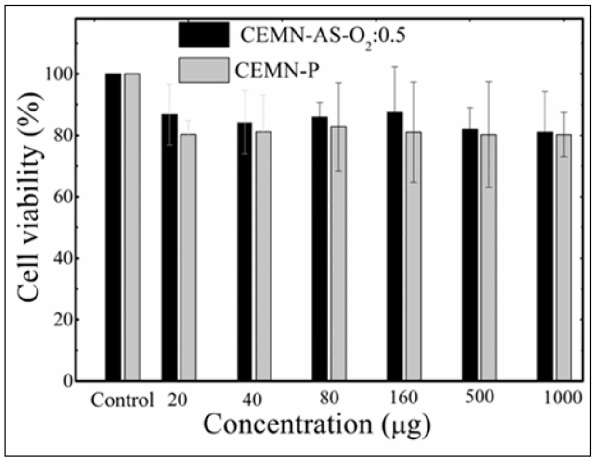

Fig.7. Cytotoxicity result for CEMN-P (0 lpm O_2) and CEMN-AS-O_2:0.5 (0.5 lpm O_2).

The prospective use of the synthesized CEMN samples in biological context requires understanding of their basic cyto-compatibility properties. In case of CEMN, the outer carbon layer will remain exposed to the immediate environment, but most of the studies in the past have concluded the graphitized nanocarbons to be mostly low toxic material in nature [26]. In a recent study for arc plasma generated carbon encapsulated Fe/Ni nanoparticles, X. fang *et al.* reported that CEMN exert excellent cyto-compatibility upto 0.1 mg/ml concentration; however significant cytotoxicity was observed beyond 1 mg/ml concentration to human breast adenocarcinoma cell-line [16]. In this paper, we investigated cyto-compatibility response of the two most important CEMN samples, CEMN-P and CEMN-AS-O2:0.5 on mouse fibroblast cell line L929 using MTT assay. Results are presented in Fig.7, where the cell viabilities for both of the nanomaterials were around 80% up to 1.6 mg/ml concentrations, indicating sufficiently good cyto-compatibility. We tested the cyto-compatibility of both the samples at higher dosages up to 10 mg/ml concentrations and observed no further decrease in cell viability. The superior cyto-compatibility of CEMN is presumably due to the presence of the outer carbon layer that fully envelopes the inner metal particles, which we know may be toxic if remain exposed [26]. CEMN-AS-O2:0.5 showed slightly higher cyto-compatibility than the CEMN samples, consistently for different dose concentrations. It is reported that in contrast to graphene, graphene-oxide is more hydrophilic in nature that can be dispersed more easily in water to form stable colloids, which in turn may enhance its biocompatibility properties [27]. This may explain the relatively better cytotoxic properties as demonstrated by the CEMN-AS-O_2:0.5 sample, because the surface of the same was functionalized with oxygen atoms.

4. Conclusions

This paper reports on the synthesis of finest carbon-encapsulated magnetic nanoparticles with narrow size distribution, through simple control of ambient pressure in the sample collection chamber, through a supersonic plasma jet assisted, fast, high-throughput process. The size control was translated into achieving superparamagnetic CEMN with one of the smallest coercive fields (7.4 Oe), which may be ideal for targeted drugs delivery and water treatment applications. The magnetic nanoparticles were tightly encapsulated by one of the thinnest surface layers so far, comprised of just one or two sheets of graphitized carbon. This could successfully protect the core from oxidation/acid-purification process and also curb the typical toxic effect of the core metal particles. The ultrathin carbon will also ensure that effective reactivity of the inner metal particles will reduce only marginally during water treatment processes. An important observation was, in contrast to the previous experiments, here the saturation magnetization of the CEMN had enhanced with reduction of pressure. In this lowest pressure regime, the highly under-expanded plasma had engulfed the substrate and burnt down the mixed carbon matrix, thus enhancing the effective magnetic moment of the synthesized nanomaterial. Another sample was processed with controlled reaction with oxygen in the sample collection chamber, with almost similar characteristics as the purified sample reported above. However, this as-synthesized sample had the advantage of being processed by a single step process, which may be especially more attractive for water

treatment applications. Both of the synthesized nanomaterial samples exhibited satisfactory cyto-compatibility properties.

Acknowledgements

We acknowledge Director, IPR for supporting this line of experiments. The first author acknowledges University Grant Commission, New Delhi, India for a fellowship under Faculty Development Program and Jagiroad College Authority, Jagiroad, Assam (India) for their kind support. She also specially acknowledges the XRD facility in the department of physics, IIT, Guwahati purchased under DST, FIST project. We are thankful to K. Deka (Tradesman B, CIMPLE- PSI Laboratory, CPP-IPR) for his continuous technical support. Support from DST, New Delhi for an experiment at PETRA III is thankfully acknowledged. This experiment was financially supported under DAE XII five-year plan projects (A30701-I & II).

References

[1] Q. A. Pankhurst, J. Connolly, S. K. Jones, J. Dobson, Application of magnetic nanoparticles in biomedicine, J. Phys. D: Appl. Phys. 36 (2003) R167-R181.

[2] X. Qu, P. J. J. Alvarez, Q. Li, Applications of nanotechnology in water and wastewater treatment, Water Res. 47 (2013) 3931-3946.

[3] R. Sergiienko, E. Shibata, A. Zentaro, D. Shindo, T. Nakamura, G. Qin, Formation and characterization of graphite-encapsulated cobalt nanoparticles synthesized by electric discharge in an ultrasonic cavitation field of liquid ethanol, Acta Mater. 55 (2007) 3671-3680.

[4] C. T. Yavuz, J. T. Mayo, W. W. Yu, A. Prakash, J. C. Falkner, S. Yean, L. Cong, A. Kan, H. J. Shipley, M. Tomson, D. Natelson, V. L. Colvin, Low-field magnetic separation of monodisperse Fe_3O_4 nanocrystals, Science 314 (2006) 964-967.

[5] Z. H. Wang, Z. D. Zhang, C. J. Choi, B. K. Kim, Structure and magnetic properties of Fe(C) and Co(C) nanocapsules prepared by chemical vapor condensation, J. Alloys Compd. 361 (2003) 289-293.

[6] J. N. Wang, L. Zhang, F. Yu, Z. M. Sheng, Synthesis of carbon-encapsulated magnetic nanoparticles with giant coercivity by a spray pyrolysis approach, J. Phys. Chem. B 111 (2007) 2119-2124.

[7] M. Bystrzejewski, A. Huczkoa, H. Lange, S. Cudzilo, W. Kicinski, Combustion synthesis route to carbon-encapsulated iron nanoparticles, Diam. Relat. Mater. 16 (2007) 225-228.

[8] N. Aomoa, T. Sarmah, U.P. Deshpande, V. Sathe, A. Banerjee, T. Shripathi, V. R. Reddy, N.P. Lalla, A. Gupta, R. Gupta, D.N. Srivastava, R.K. Bordoloi, S. Sarma, A. Srinivasan, M. Kakati, Plasma-assisted synthesis of carbon encapsulated magnetic nanoparticles with controlled sizes correlated to smooth variation of magnetic properties, Carbon 84 (2015) 24-37.

[9] J. Borysiuk, A. Grabias, J. Szczytko, M. Bystrzejewski, A. Twardowski, H. Lange, Structure and magnetic properties of carbon encapsulated Fe nanoparticles obtained by arc plasma and combustion synthesis, Carbon 46 (2008) 1693-1701.

[10] J. B. Park, S. H. Jeong, M. S. Jeong, J. Y. Kim, B. K. Cho, Synthesis of carbon-encapsulated magnetic nanoparticles by pulsed laser irradiation solution, Carbon 46 (2008) 1369-1377.

[11] M. Bystrzejewski, S. Cudziło, A. Huczko, H. Lange, G. Soucy, G. Cota-Sanchez, W. Kaszuwara, Carbon encapsulated magnetic nanoparticles for biomedical applications: Thermal stability studies, Biomol. Eng. 24 (2007) 555-558.

[12] W.K. Oh, H. Yoon, J. Jang, Size control of magnetic carbon nanoparticles for drug delivery, Biomaterials. 31 (2010) 1342-1348.

[13] M. Bystrzejewski, Z. Károly Z, J. Szépvölgyi J, A. Huczko, H. Lange, Continuous synthesis of controlled size carbon-encapsulated iron nanoparticles, Mater. Res. Bull. 46 (2011) 2408-2417.

[14] I. Morjan, F. Dumitrache, R. Alexandrescu, C. Fleaca, R. Birjega, C.R. Luculescu, I. Soare, E. Dutu, G. Filoti, V. Kuncser, G. Prodan, N.C. Popa, L. Vékás, Laser synthesis of magnetic iron–carbon nanocomposites with size dependent properties, Adv. Powder Technol. 23 (2012) 88-96.

[15] M. Bystrzejewski, O. Łabedź, W. Kaszuwara, A. Huczko, H. Lange, Controlling the diameter and magnetic properties of carbon-encapsulated iron nanoparticles produced by carbon arc discharge, Powder Technol. 246 (2013) 7-15.

[16] X. Fang, X. Cheng, Y. Zhang, L.G. Zhang, M. Keidar, Single-step synthesis of carbon encapsulated magnetic nanoparticles in arc plasma and potential biomedical applications, J. Colloid Interface Sci. 509 (2018) 414-421.

[17] M. Dickinson, T.B. Scott, The application of zero-valent iron nanoparticles for the remediation of a uranium-contaminated waste effluent, J. Hazard. Mater. 178 (2010) 171-179.

[18] D. Zhang, S. Wei, C. Kaila, X. Su, J. Wu, A. B. Karki, D. P. Young, Z. Guo, Carbon-stabilized iron nanoparticles for environmental remediation, Nanoscale 2 (2010) 917-919.

[19] M.J. Wozniak, P. Wozniak, M. Bystrzejewski, S. Cudzilo, A. Huczko, P. Jelen, W. Kaszuwara, J.A. Kozubowski, H. Lange, M. Leonowicz, M. Lewandowska-Szumiel, Magnetic nanoparticles of Fe and Nd-Fe-B alloy encapsulated in carbon shells for drug delivery systems: Study of the structure and interaction with the living cells, J. Alloys Compd. 423 (2006) 87-91.

[20] I.P. Grudzinski, M. Bystrzejewski, M.A. Cywinska, A. Kosmider, M. Poplawska, A. Cieszanowski, A. Ostrowska, Cytotoxicity evaluation of carbon-encapsulated iron nanoparticles in melanoma cells and dermal fibroblasts, J. Nanoparticle Res. 15 (2013) 1835.

[21] I.P. Grudzinski, M. Bystrzejewski, M.A. Cywinska, A. Kosmider, M. Poplawska, A. Cieszanowski, Z. Fijalek, A. Ostrowska, Comparative cytotoxicity studies of carbon-encapsulated iron nanoparticles in murine glioma cells, Colloids Surf., B 117 (2014) 135-143.

[22] M. Kakati, B. Bora, U. P. Deshpande, D. M. Phase, V. Sathe, N. P. Lalla, T. Shripathi, S. Sarma, N. K. Joshi, A. K. Das, Study of a supersonic thermal plasma expansion process for synthesis of nanostructured TiO_2, Thin Solid Films 518 (2009) 84-90.

[23] A. Hasan, G. Waibhaw, S. Tiwari, K. Dharmalingam, I. Shukla, L.M. Pandey, Fabrication and characterization of Chitosan, polyvinylpyrrolidone and cellulose nanowhiskers nanocomposite films for wound healing drug delivery application, Journal of Biomedical Materials Research Part A 105 (2017) 2391-2404.

[24] S. Ravi, P. Silva, S. Xu, B.X. Tay, H.S. Tan, W.I. Milne, Nanocrystallites in tetrahedral amorphous carbon films, Appl. Phys. Lett. 69 (1996) 491.

[25] S.C.N. Tang, I.M.C. Lo, Magnetic nanoparticles: Essential factors for sustainable environmental applications, Water Res. 47 (2013) 2613-2632.

[26] J. Liu, L. Cui, D. Losic, Graphene and graphene oxide as new nanocarriers for drug delivery applications, Acta Biomater. 9 (2013) 9243-9257.

[27] I. Dulinska-Molak, A. Chlanda, J. Li, X. Wang, M. Bystrzejewski, N. Kawazoe, G. Chen, W. Swieszkowski, The influence of carbon-encapsulated iron nanoparticles on elastic modulus of living human mesenchymal stem cells examined by atomic force microscopy, Micron (2018). (In press, accepted manuscript)

Supplementary Materials

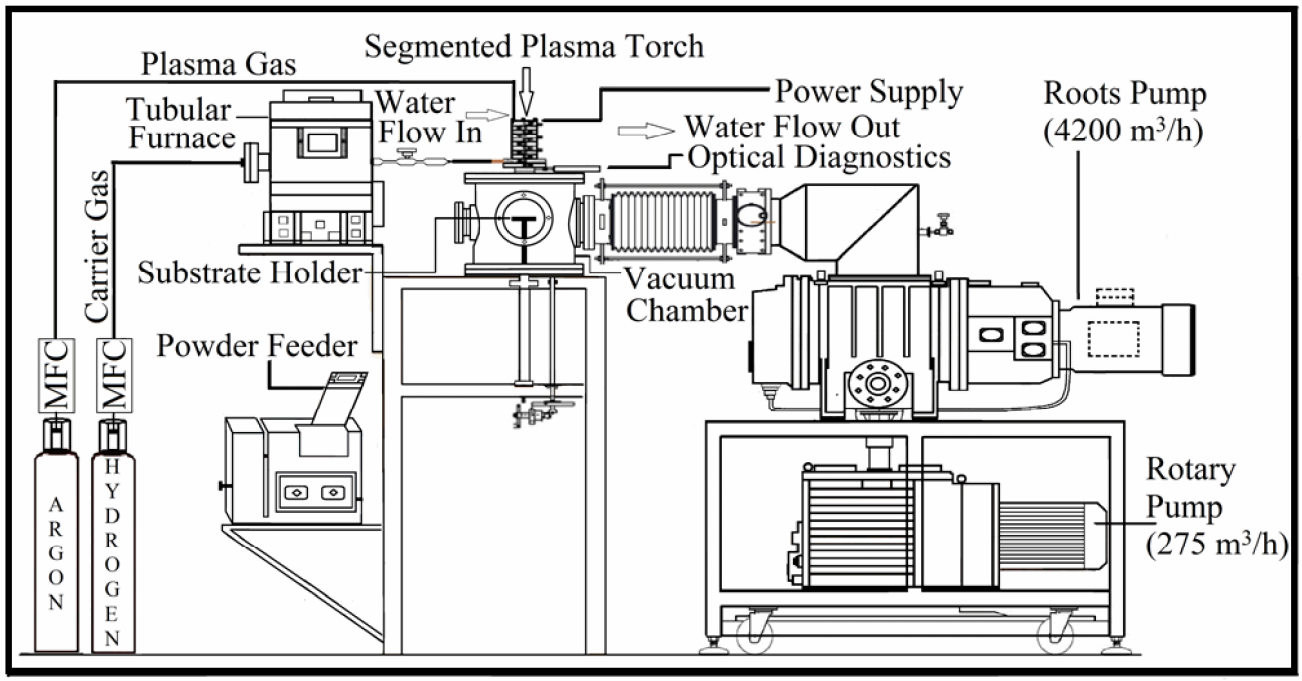

Figure S1: The segmented plasma torch assisted experimental nanoreactor system.

- Controlled plasma synthesis of C encapsulated superparamagnetic nanoparticles.
- Small angle X-ray scattering confirms 5 nm size and ultrathin carbon coating.
- VSM measures 67 emu/g saturation magnetization and 7.4 Oe coercive field.
- Controlled plasma heating at low pressure burns-off extra carbon.
- Nanomaterials likely to be ideal for biomedical and environmental applications.